FULL-SCALE TUNNEL EXPERIMENTS FOR FUEL CELL HYDROGEN VEHICLES: JET FIRE AND EXPLOSIONS

BOUIX D.[1], SAUZEDDE F. [1], MANICARDI P. [1], MARTIN M. [1], FORERO-MORENO D. M. [2], STUDER E. [2], BERNARD-MICHEL G. [2], KOUDRIAKOV S. [2], GUEGUEN H. [2], POURRE BRICHOT P. [2], DENAGTERGAEL A. [2], DOMERGUE L. [2].

[1] DEHT, CEA, Grenoble, France

[2] CEA, Université Paris-Saclay, Saclay, France.

ABSTRACT

In the framework of the HYTUNNEL-CS European project sponsored by FCH-JU, a set of preliminary tests were conducted in a real tunnel in France. These tests are devoted to safety of hydrogen-fueled vehicles having a compressed gas storage and Temperature Pressure Release Device (TPRD). The goal of the study is to develop recommendations for Regulations, Codes and Standards (RCS) for inherently safer use of hydrogen vehicles in enclosed transportation systems. Two scenarios were investigated, (a) jet fire evolution following the activation of TPRD due to conventional fuel car fire, and (b) explosion of compressed hydrogen tank. The obtained experimental data are systematically compared to existing engineering correlations. The results will be used for benchmarking studies using CFD codes. The hydrogen pressure range in these preliminary tests has been lowered down to 20MPa in order to verify the capability of various large-scale measurement techniques before scaling up to 70 MPa, the subject of the second experimental campaign.

1.0 INTRODUCTION

Hydrogen Fuel Cell Electric Vehicles (HFC EVs) represent an alternative to current internal combustion engine vehicles. The use of these vehicles with storage of compressed gaseous hydrogen (CGH2) or cryogenic liquid hydrogen (LH2) in confined spaces, such as tunnels, underground car parks, etc., creates new challenges to ensure the protection of people and property and to keep the risk at an acceptable level. Several studies have shown that confinement or congestion can lead to severe accidental consequences compared to accidents in an open atmosphere. It is therefore necessary to develop validated hazard and risk assessment tools for the behavior of hydrogen in tunnels. The HYTunnel-CS project sponsored by the FCH-JU pursues this objective. Among the experiments carried out in support of the validation, the CEA is conducting full-scale tests inside a road tunnel.

In the past, hydrogen gas explosion in a tunnel-like geometry have been carried out by SRI (Stanford Research Institute) at the Corral Hollow Experiment Site **[1]** in order to compare the behavior with open field experiments. This is a scaled-down facility. The tube representing the tunnel is 78.5 m long and has a diameter of only 2.4 m. It has an embankment in the lower part, which gives it a horseshoe shaped cross-section of 3.74 m². Sato et al. **[2]** describe hydrogen explosion experiments in this facility corresponding to TPRD release scenarios for cars or buses but also to leaks on bottled hydrogen transports. The released gas mixture is ignited at the end of the release at the top of the tunnel and above the release. The overpressures measured along the tunnel are relatively low. The maximum value is 2 mbar for an ATEX (Atmosphère Explosive, or EXplosive ATmosphere) corresponding to a release of 1.8 m^3 of hydrogen (144 g) in 35 seconds (scaled from the tanks of a bus at 350 bar). The overpressure is relatively constant along the 40 m of the tunnel. In the same facility, Groethe et al. **[3]** report the results of tests with homogeneous ATEX located in the center of the tunnel (37 m^3 or about 13% of the total volume). At 9.5% hydrogen, the overpressures are not detected by the measurements. Higher hydrogen gas concentrations, i.e. 20% (670 g of hydrogen) produce an overpressure of about 350 mbar and 30% (~1 kg) produce 1500 mbar. There is negligible reduction in overpressure along the tunnel. Obstacles such as cars (3% blockage ratio) do not change the above overpressure values. Transient releases representing vehicle leakage scenarios (at the tunnel scale 100 g in 20s and 2.2 kg in 420s) carried out in the case of ventilation (1.6 m^3/s, i.e. a wind speed of about 0.5 m/s) did not ignite or gave

overpressures below the measurement threshold. More recently, Houf at al. **[1]** describe experiments carried out in the same facility but for a scenario corresponding to the simultaneous opening of three TPRDs under a vehicle. The latter is represented in the installation by a hexahedron. Pre-calculations of these tests showed that the maximum overpressure is obtained, for an ignition at the ceiling above the release, after 10 seconds of release whereas the maximum volume of the ATEX is expected after 20 seconds. The tests confirmed this point with a maximum overpressure of 500 mbar after about 2 seconds of release (scale factor). Many other numerical simulations are available in the literature i.e. Venetsanos et al. **[4]**, Middha et al. **[5]**, Bie et al. **[6]** and Li et al **[7]**. Restricting ourselves to scenarios involving cars with a 700 bar pressure tank without ventilation (worst case), Venetsanos et al. analyzed the combustion with ignition when the size of the flammable cloud was the largest (t=20 s, 519 m^3 of ATEX and 3.73 kg of hydrogen inside). The ignition was located above the release near the ceiling. The calculated overpressures are 23 mbar in the near field and 10 mbar at 100 m. The fireball created by the combustion extends over 47 m. Middha et al. also ignite the mixture when the volume of the ATEX is larger but they define an equivalent stoichiometric volume (4.4 m^3 with 70 g of hydrogen if the TPRD discharges upwards and 17.8 m^3 with 290 g of hydrogen, if it is directed downwards). In the first case, the calculated overpressures along the tunnel vary from 100 to 50 mbar, while in the second case they range from 340 to 110 mbar. The reduction over the 200 m length of the tunnel is of the order of 30%. Bie et al. are interested in the near field (+/- 10 m) and investigate ignitions at 3.1 and 6.2 seconds after the onset of release without any mention of the evolution of the size of the flammable cloud. The calculated overpressures are 100 to 130 mbar. Finally, Li et al. present combustion calculations in the case of detonation because their analyses conclude that DDT (Deflagration-to-Detonation Transition) is highly sensitive. In the near field, the overpressures are therefore extremely high, up to 10 bar, and even reach the value of 2 bar at 5 m. From this, it can be concluded that the analyses carried out do not necessarily define the worst case of ignition when the volume of ATEX is the largest. Moreover, the consequences in terms of overpressure vary from one analysis to another. Nevertheless, most of them emphasize the limited attenuation of pressure waves in the tunnel. A universal correlation for blast wave decay after hydrogen tank rupture in a tunnel fire has been developed using methods of similitude analysis and validated via numerical experiments **[8]**. The tunnels cross-section area varied from 24 m^2 to 139 m^2, aspect ratio width-height - from 1.2 to 2.7, and tunnel length - from 150m to 1500 m. The tanks of volume 15L to 176 L under pressure of 35MPa to 95 MPa were considered.

Several jet-fire experiments were performed in the past mostly in open atmosphere (see **[8]** for a review). Some large hydrogen jet-fires **[9], [10]** were carried out in a mine gallery but the flame was horizontal. These results are similar to those done in an outdoor environment and therefore the confinement created by the gallery has no significant effect. Kuznetsov et al **[11]** performed hydrogen jet-fires in a confined volume at a reduced scale (~1m^3). Well-ventilated as well as under-ventilated conditions were experienced according to the size and position of the vents. Limiting access to the oxidant can lead to oscillations of the flame between the inside and outside of the volume; the condensation of water vapor having a strong influence in this case. The simulations carried out on these tests have provided a clear understanding of the behavior of the jet-fire in a vented enclosure. Finally, Li et al. **[7]** carried out numerical simulations of ignited upward release in a road tunnel. The jet flame is confined by the tunnel ceiling and grows under it. Initially it expands but as the flow rate decreases it shrinks back towards the release point. A large Heat Release Rate (up to 43 MW) is predicted a few seconds after the start of the release but unlike a conventional vehicle, the duration of the phenomenon is short and the consequences are therefore limited to the vicinity of the release and locally to the tunnel ceiling. We conclude that in all these cases, there is limited number of experimental data for model validation and especially no full-scale data.

In the present article, which deals with jet-fire and tank rupture in full-scale tunnel geometry, the first part is devoted to the description of the geometry of the tunnel and the system used to simulate the HFC-EV and to produce the jet-fire. In the same section, the method used to burst the pressurized tanks is described. Then, the measurement devices are detailed in order to follow the jet-fire transient and the pressure waves along the tunnel. The third part provides details of the experimental data and gives some comparisons with simulation results. Conclusions follow. The article only takes into account the pre-

tests carried out with a maximum pressure inside the cylinder of 200 bar but a second campaign with a maximum pressure of 700 bar is to be carried out in June and the main results will be added during the presentation at the conference.

2.0 GEOMETRY, MEASUREMENTS AND TEST SEQUENCES

2.1 TUNNEL GEOMETRY, GAS RELEASE DEVICE AND TANK RUPTURE METHODOLOGY

The experiments were carried out in the Tunnel du Mortier located in the commune of Autrans in the Vercors, France (Figure 1). This tunnel is 507 m long and is a disused straight road tunnel in the shape of a horseshoe. On the entrance (on Autrans side) the vault is concreted (Images 1 and 2) while the inside of the tunnel is in rough rock image 3 and 4). The concrete section is 133 m long, 7.5 m wide and 5.2 m high. The rocky area represents the rest of the length with a width of 8.9 m and a height of 5.6 m. The slope is 3.6% and there is no mechanical ventilation. Finally, another concrete section is located at the exit of the tunnel.

The jet-fire tests were conducted 72 m from the entrance to the concrete section and the tank rupture tests were performed in the rocky part, 212 m away from the upper entrance. Two straw walls were installed at each end of the tunnel to limit natural convection, which could vary greatly from one day to another, depending on weather conditions, and to quench the pressure waves. Under these conditions, all the tests were practically carried out with a wind speed inside the tunnel of about 0.3-0.4 m/s from top to bottom.

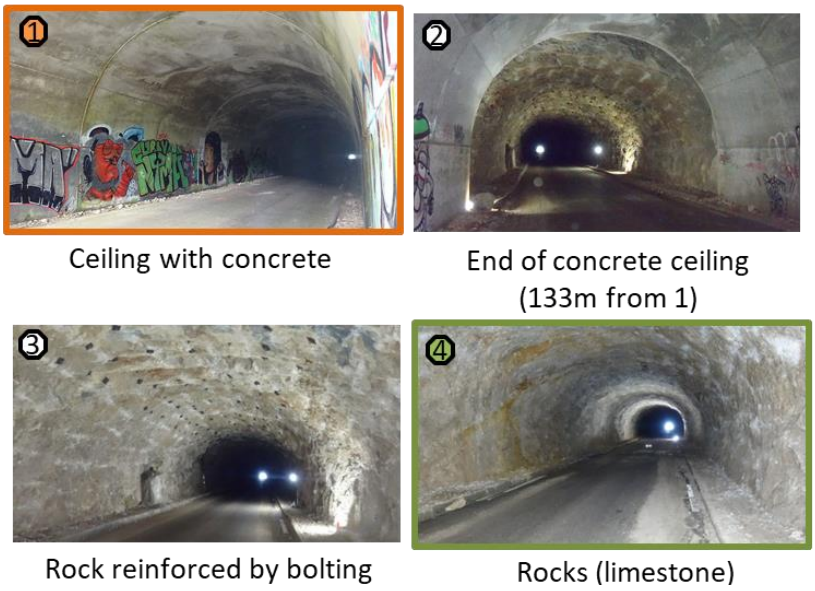

Figure 1. Tunnel geometry

The system used to simulate an HFC-EV vehicle has been described in the companion paper. It consists of a horizontal plate 4.5 m long and 1.9 m wide representing the chassis of the car (Figure 2). This chassis is positioned centrally in the tunnel for reasons of symmetry and is 21.5 to 23.5 cm above road level. A type 2 cylinder of volume close to 50 litres at 200 bar pressure represents the tank. The discharge is performed by a Thermally activated Pressure Relief Device (TPRD) located opposite to the tank at 15 cm from the end of the chassis for safety reasons. This TPRD can be oriented towards the ground or towards the vault. Different diameters varying between 0.5 and 3 mm have been considered. The glass bulb contained in the TPRD was broken beforehand and the discharge coefficients (CD) of the orifice

were also qualified in dedicated nitrogen experiments. Particular attention has been paid to this injection system to avoid any diameter restriction and to guarantee a very low-pressure drop between the cylinder and the upstream side of the TPRD. A small propane Meker burner located above the chassis nearby the TPRD release ignites the jet-fire.

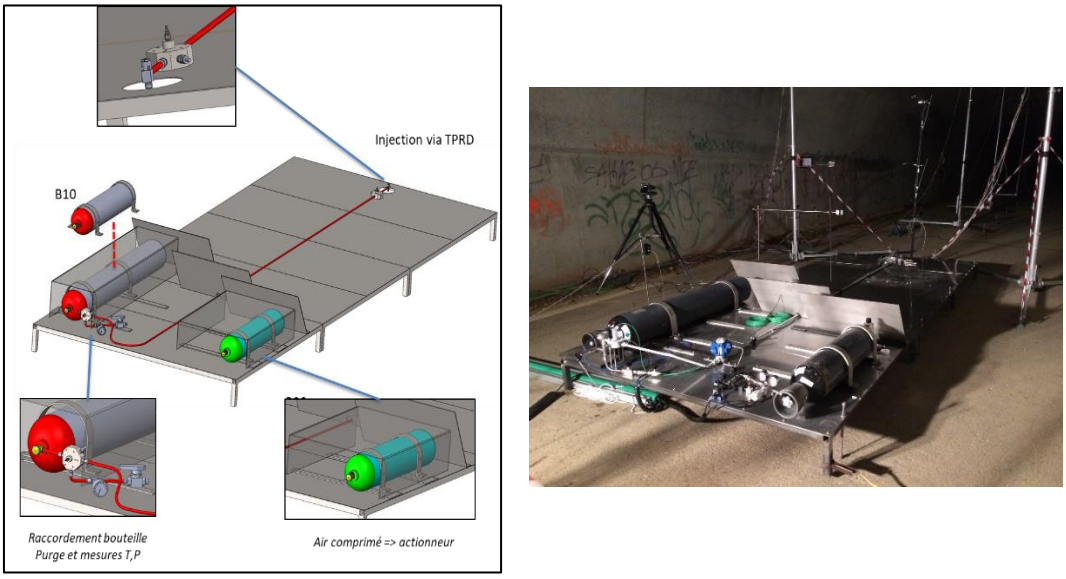

Figure 2. Gas release device

A large propane square burner (Leader PYROS 3 - wet) has been installed nearby the chassis (along the tunnel axis) in order to simulate a conventional fueled-car fire, which is supposed to be the initiator of TPRD opening (Figure 3). It has a firebox area of 0.83 m² and a power output of up to approx. 800 kW. In the tests we measured the propane flow rate to the burner (Brooks mass flow-controller).

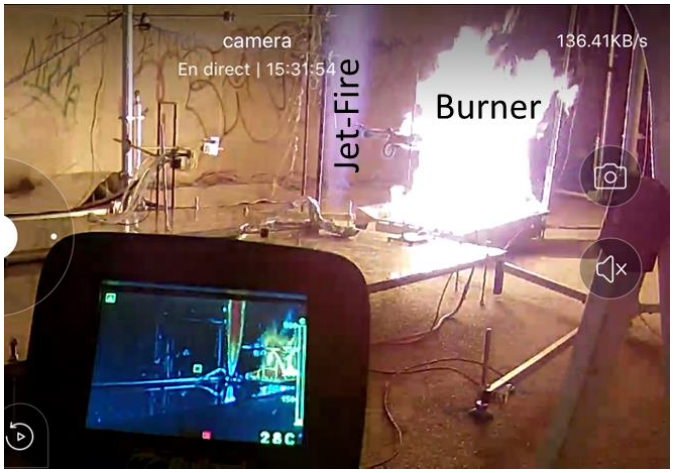

Figure 3. Jet-fire and burner arrangement.

Pressurized tank rupture experiments were conducted in order to study several points: the decay of blast waves in a tunnel-type geometry and the proportion of chemical energy to be added to mechanical energy to evaluate the source term following a tank explosion. Usually, the tank is set on fire and if there is no depressurization means, the tank ends up exploding. In order to simplify the procedure and guarantee reproducibility, we have chosen to open the pressurized tank using a detonation belt

(RAZOR). This belt is located at the middle of the tank and a small sphere of explosive located in the upper part initiates its explosion (Figure 4 - left). As far as possible, we tested the tanks with two different gases: helium or hydrogen. Systematically, for each tank, after the first explosion we kept a fragment and re-tested it with the detonating belt alone to measure its contribution (Figure 4 - right). Type 2, 3 and 4 tanks were used for these tests with different inner volumes.

Figure 4. Tank rupture method.

2.2 MEASUREMENT TECHNIQUES

The tank blow-down measurements have already been described in the companion paper and the pressure, temperature measurements provide the mass balance in the tank, and thus the mass flow rate can be deduced. Several type K thermocouples have also been installed on different vertical rods to monitor the gas temperature inside the tunnel, mostly close to the vault. Thermocouples located near the burner or jet-fire are protected from the radiative flux by a thin stainless steel plate.

During the jet-fire tests, eight heat flux sensors (Captec 30x30 mm) are set-up along a single line arrangement (Figure 5 left) facing the jet-fire. The burner cannot be completely hidden from these heat flux sensors especially from those which are at a large distance. Two other water-cooled heat flux sensors (Medtherm 64-2-20 and Capthem) are installed close to the TPRD at 90 degrees to each other, one in the axis of the jet-fire and the burner.

In order to capture the pressure waves during the explosion tests, five PCB blast wave pencils were arranged in the tunnel at distances of 38 m, 45 m, 90 m, 142 m and 205 m from the tank. These sensors are mounted on tripods approximately 80 cm above the ground (Figure 5 right). Finally, in order to monitor the propagation of the fireball during the explosion of the tanks, a line of ten thin (0.25 mm) type K thermocouples was installed near the ceiling of the vault in the axis of the tunnel. This line extends +/- 17 m around the tank.

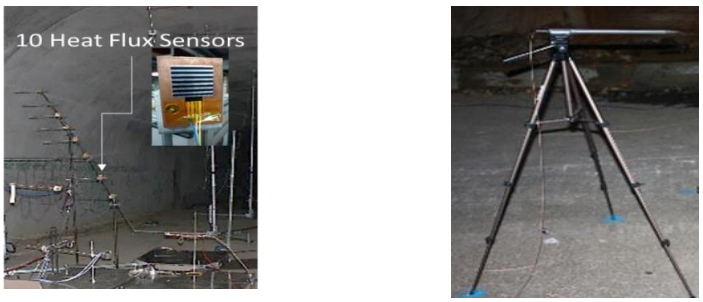

Figure 5. Specific measurement techniques. Left Heat-Flux sensors, Right PCB blast wave pencils.

2.3 TEST SEQUENCES

During the jet-fire tests, the diameter of the TPRD as well as its orientation were varied as shown in Table 1. We also reported the climatic conditions in the tunnel just before the tests as well as the duration of the discharge phase. Some of the tests have been repeated twice in order to check the reproducibility. The effect of the burner operation on the jet-fire fire behavior has also been assessed. During the tests, the burner is turned-on approximately 5 minutes before the start of the jet-fire and the Heat Release Rate is close to 400 kW.

Table 1. Jet-fire Test sequences.

Test Number	TPRD diameter (mm)	TPRD Orientation	Initial Pressure (bar)	Initial temperature (°C)	Initial RH (%)	Duration of blow-down phase (s)	Burner
15	No	-	0.865	7.2	85.	-	Yes
16*	0.5	Upward	0.869	8.0	86.	1500*	No
17	2	Upward	0.868	8.6	89.	176	No
18	3	Upward	0.868	8.8	88.	84	No
19	3	Upward	0.868	8.7	82.	82	Yes
20	2	Upward	0.868	9.7	80	192	Yes
21	2	Upward	0.867	10.0	81.	198	Yes
22	2	Downward	0.867	10.0	85.	191	No
23	2	Downward	0.867	8.9	89.	193	Yes

*Some sensors were damaged during the test

Tank rupture test matrix is provided in Table 2.

Table 2. Tank rupture Test sequences.

Tank type	Tank volume (l)	Gas inside	Gas pressure (bar)	Gas temperature (°C)	Explosive belt charge (g TNT)	Mechanical Energy (g TNT)
Tank 1	150	Helium	41	5.0	200	215
Tank 2	50	Hydrogen	47	5.0	270	134
Fragment Tank 2	---	---	---	---	270	---

3.0 TEST RESULTS

3.1 JET-FIRE EXPERIMENTS

First, from the videos of the jet-fire alone, we carried out an image processing to have the geometry of the flame, visible length and width, as a function of time (Figure 6 - left). The width represents about 17% **[13]** of the length and the comparison with the most recent correlation from the work of Molkov et al. [8] gives acceptable results as this correlation was established from open fires and is slightly conservative (Figure 6 - right). Initially, our experimental values are well below the corresponding values of the correlation, which probably reflects the effect of tunnel confinement (5 m between TPRD and top of the vault).

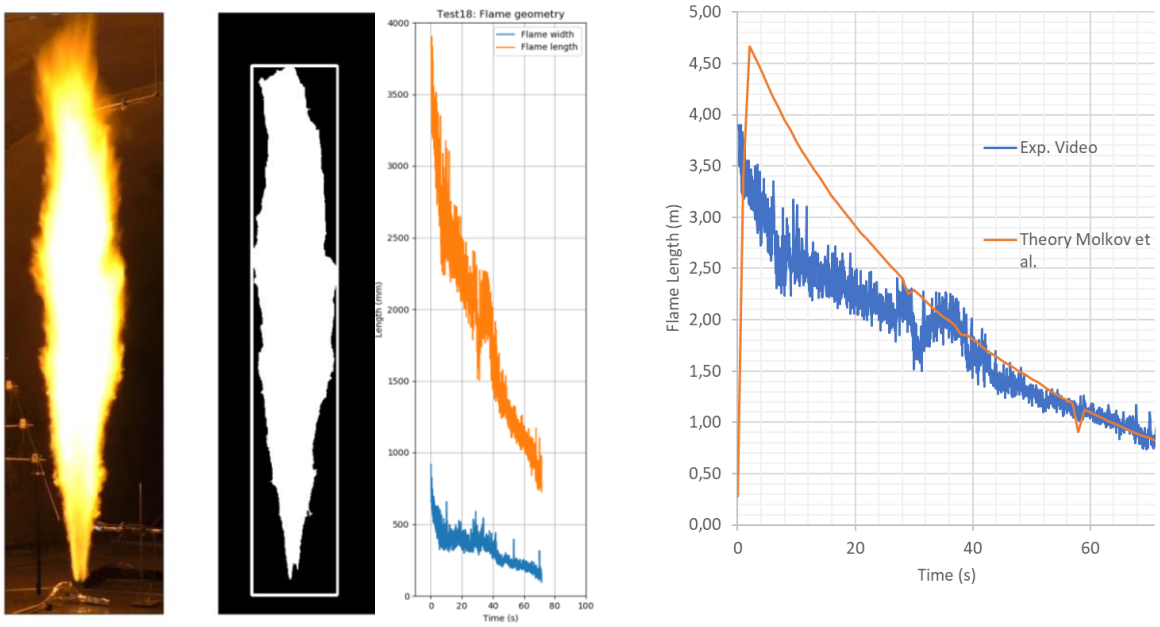

Figure 6. Test 18: Visible flame length and width. Left – Experiments Visible flame, binarized flame, and bounding box sizes, Right - comparison of visible flame length with theory.

Next, we studied the radiative flux emitted by the hydrogen flame. Our measurements are first compared with the model of Schefer et al [13] assuming a point source. For the sensor located at r=2 m and z=2 m with respect to the TPRD (Figure 7 – Left), the experiment is well below the model, which can be explained by the fact that this sensor is in the near field and therefore the point source hypothesis is no longer valid. For the sensor located further away (r=3 m and z=3 m, Figure 7 - Right), the point source model matches better. We also compared our results with the multipoint source model proposed by Hankinson et al. [14]. With this model, the radiative flux measured by the sensor in the near field is better predicted.

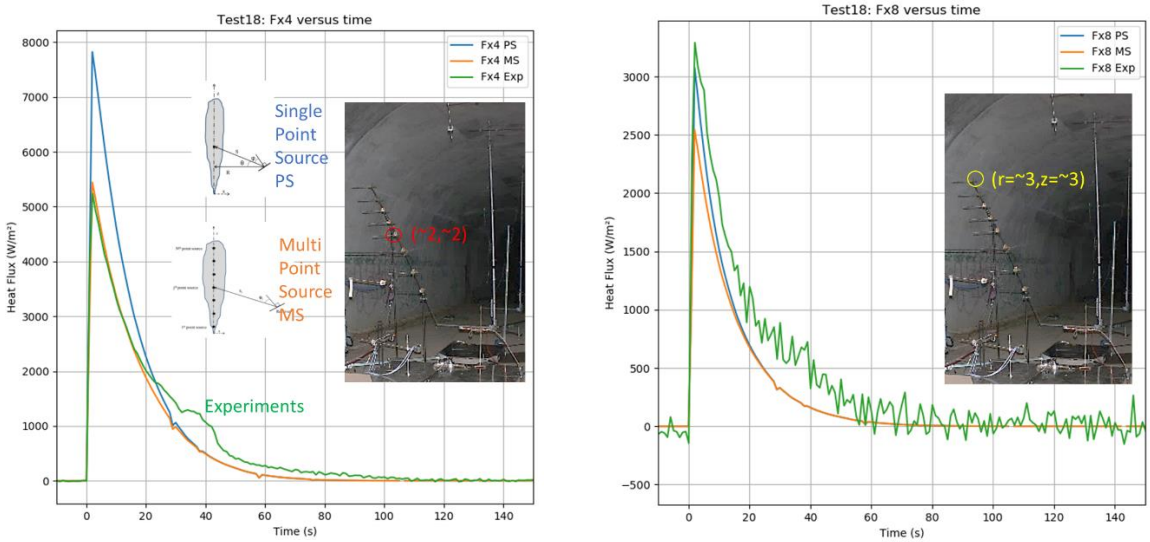

Figure 7. Test 18: Radiative heat flux. Left – radiometer located at (2,2), Right - radiometer located at (3,3).

Another important result of these tests is the effect of the TPRD diameter on the jet-fire. As shown in Figure 8, the temperature of the combustion products of the hydrogen flame measured near the top of the vault decreases sharply with the diameter of the TPRD. The same phenomenon is observed for the

radiated fluxes. It should also be mentioned that the duration of the blow-down phase increases as the diameter of the TPRD is reduced. Consequently, the thermal doses increase and there is necessarily an optimum to be found with regard to the consequences.

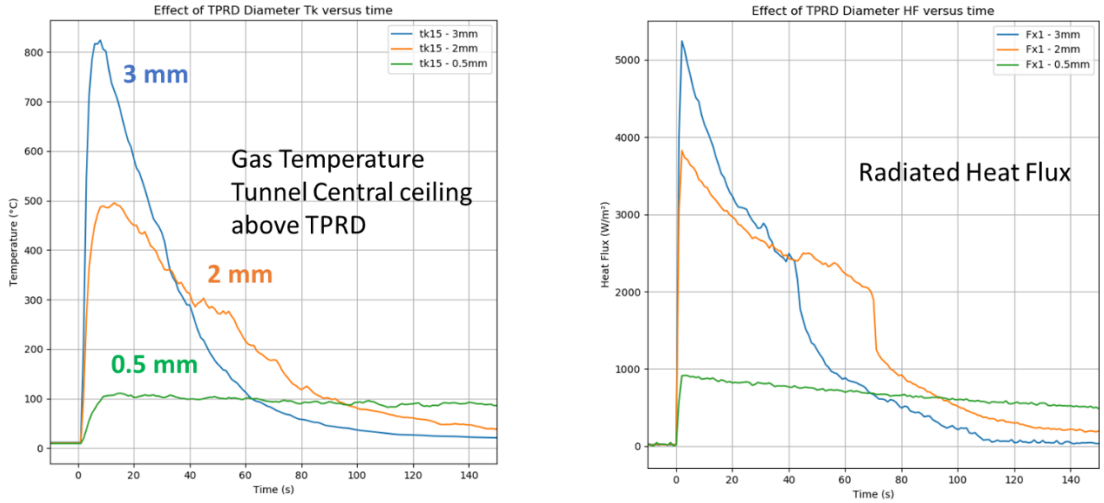

Figure 8. Effect of TPRD diameter. Left – Gas temperature near the top of the vault above the jet-fire, Right – Radiative heat flux at (3,3).

Then, when coupled with the burner, the most important effects were observed in the downward discharge. The air entrained by the burner flames is strongly disturbed by the jet-fire. However, the differences in the measurements are small. Finally, we carried out reproducibility tests (20 and 21) to demonstrate our proper control of initial and boundary conditions. Figure 9 shows that both the temperature and heat flow data are perfectly reproducible.

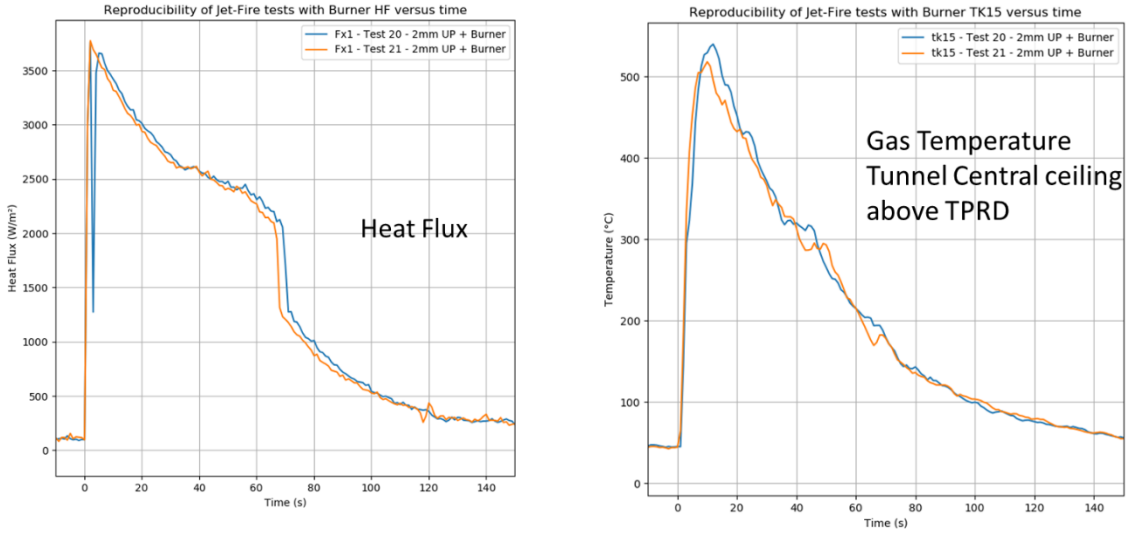

Figure 9. Reproducibility of jet-fire tests.

3.2 TANK EXPLOSION EXPERIMENTS

Pressure decay along the tunnel

The results of three main tests will be described in this paper (Table 2). Two different tanks were used during this preliminary test campaign (Figure 10). Tank 1 (Figure 2, left) is a Type 3 150-litre capacity cylindrical tank. It has a protective fiberglass outer layer. One end of the Tank is in the form of a dome equipped with fittings for filling. The Tank 2 (Figure 10, middle) is Type 2 50-litre capacity cylindrical tank. Both tanks were open with flexible linear shaped charges of RAZOR model. The test initial conditions are given in Table 2. Additional test was conducted where the fragment of the Tank 2 was opened with explosive belt having the same charge as the one used for the opening of the hydrogen-filled tank, i.e. 270 g of TNT (Figure 10, right). This is done in order to estimate the contribution of the explosive belt charge to the blast wave strength.

Figure 10. Tank 1 (left), Tank 2 (middle) and a fragment of Tank 2 (right) prior to Tests

The blast wave propagation inside a tunnel is qualitatively described in [15] where a series of computations has been performed using different tunnel geometries. At initial stage, before reaching the closest wall, the blast wave has a hemispherical shape. After that, the blast wave is reflected from the tunnel walls, and the multiple reflections can be observed on the pressure signals. Later on, at a certain distance from the explosion, the secondary waves coalesce with the leading front and the resulting blast wave propagates as a planar structure. We can therefore separate the blast wave run-up distance on *Zone 1*, where pressure signals are dominated by reflections, and *Zone 2*, where planar structure of blast wave is observed.

Let us consider the overpressure temporal evolutions corresponding to the explosions of Tank 1 (orange curve), Tank 2 (blue curve), and fragments of Tank 2 (green curve) using detonation belts (Figure 11). The pressure signals of the Tank 1 explosion and of Tank 2 fragment explosion are shifted in time, +5.42ms and +2.17ms, respectively, for better comparison. Inside the Zone 1 the first pressure peak is due to explosion of the small sphere that initiates the detonation belt explosion. For the three cases considered here, these overpressure peak values are identical. The second pressure peak is the result of the explosion of the detonation belt. Again, for the two distances considered, 38 m and 45 m, the maximum peak overpressures are very similar. What is interesting is that the overpressure signal from explosion of Tank 1 containing helium gas is very similar, in terms of a period and amplitude, to the overpressure signal corresponding to the explosion of a fragment of Tank 2. The overpressure evolution resulting from explosion of the hydrogen filled Tank 1 shows higher amplitudes for $t > 0.12$ s, compare to the previous two signals. This is expected, as there is a contribution of chemical energy due to hydrogen burning. The period of oscillations of the above-described pressure signals varies between 12 ms and 20 ms. We mention that in the Zone 1, the width and the height of the tunnel are 5.6 m and 8.9 m, respectively. This gives us time scales of 16.7 ms and 26.6 ms (we take speed of sound $c = 335$ m/s).

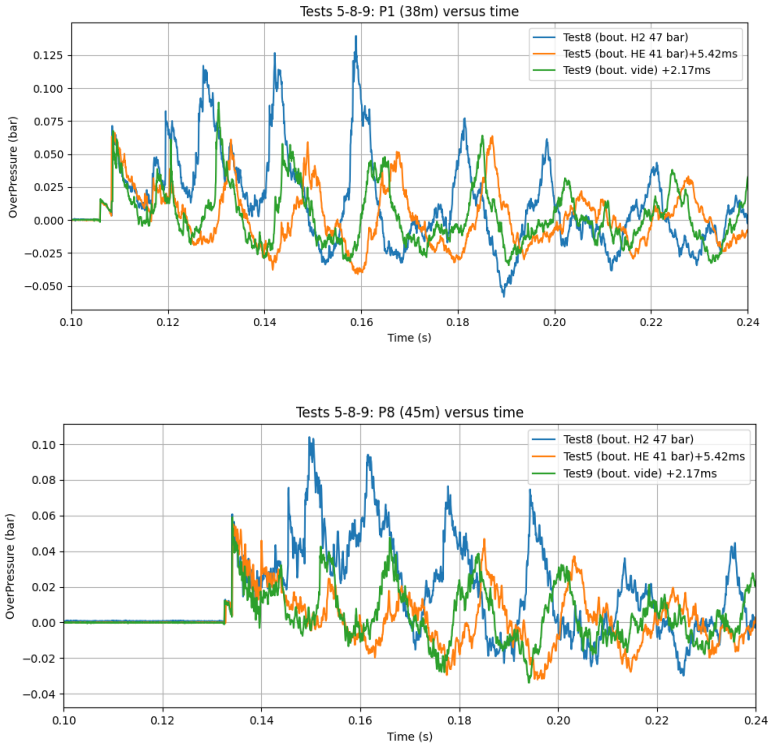

Figure 11. *Zone 1*. Overpressure evolution with time at 38 m (top) and 45 m (bottom) from explosion. GH2 means “Gaseous Hydrogen”, GHE – “Gaseous Helium”, DB – “Detonation Belt”.

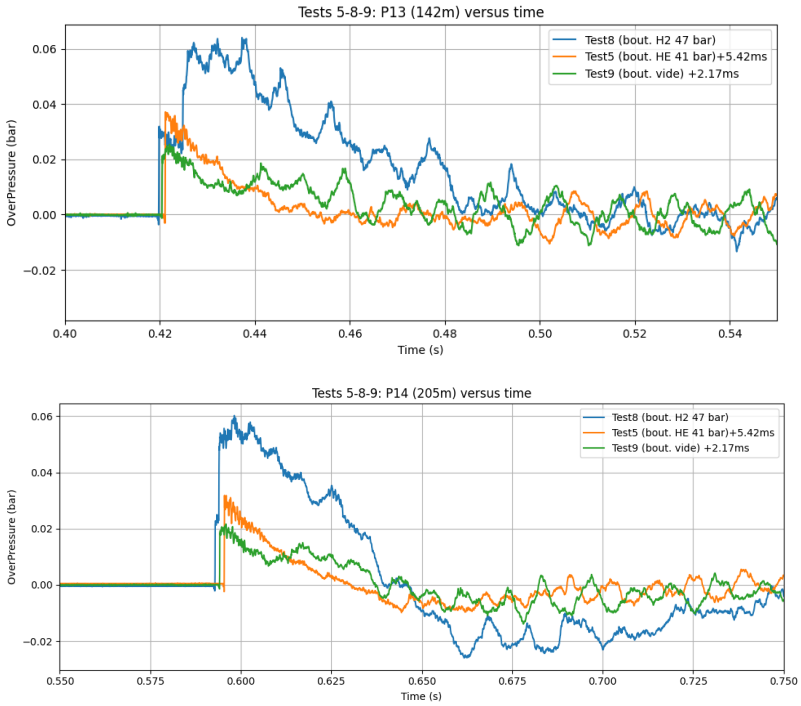

Figure 12. *Zone 2*. Overpressure evolution at 142 m (top) and at 205 m (bottom) corresponding to GH2 (blue curve), GHE (orange curve) and DB (green curve).

The overpressure evolutions at distances 142 m and 205 m from explosion reveal different behaviour (Figure 12). The pressure resembles more to a planar front, especially at 205 m. If we focus on hydrogen-filled Tank 2 (blue curve), at 142 m we can still distinguish the peak corresponding to the detonation belt explosion, while at 205 m the blast wave having mechanical and chemical energy inputs catches up the blast wave initiated by the detonation belt. The contribution of the chemical energy is clearly seen; it gives the maximum overpressures which are twice more important than those corresponding to the helium-filled Tank 1 explosion. Moreover, at these distances, the contribution of the mechanical energy (orange line) is visible; in comparison with the overpressure values resulting from fragment explosion by detonation belt, the maximum pressure values are about 50% higher.

One of the important questions for the safety analysis is how to quantify the fraction of the chemical energy contained in a compressed flammable gas that would contribute to the blast wave strength. When we consider an explosion of a hydrogen-filled tank, the energy of the corresponding blast wave has contributions from three sources: (1) detonation belt explosion, (2) mechanical energy of compressed gas, and (3) chemical energy due to hydrogen combustion. We mention in passing that the first contribution is specific only to the present experimental campaign. Some part of the energy contained in a detonation belt is spent on tank opening, while some part of the mechanical energy contributes to the fragments motion. While dealing with high internal gas pressures, of the order of 700-1000 bar, one can probably neglect these energy losses. In the present pre-test campaign, the gas pressure inside the tanks was close to 40 bar and the abovementioned energy losses cannot be neglected and have to be quantified.

The following strategy is implemented in order to evaluate different energy contributions following a tank explosion.

- Preliminary tests using pure plastic explosive located on the tunnel floor, has provided us with blast wave overpressures inside the tunnel. The maximum overpressures in Zone 2 are compared favourably with the correlation of [16] for overpressure decay along the tunnel. This correlation uses TNT curve for open space detonation at ground level while scaled distance R is modified using the Energy Concentration Factor (ECF):

  $$R = \frac{r}{(ECF \cdot M)^{1/3}}; \text{ where } ECF = \frac{1}{3}\frac{\pi}{A}r^2,$$

  A is the tunnel cross sectional area, equal to 39 m2 in our case, and M is the equivalent weight of explosive charge, kg, and r is the distance for the explosion centre, m.

- We varied the mass of TNT, which serves as an input to the correlation [16], and the theoretical overpressure values were systematically compared to the maximum overpressure values from the experiment where fragment of the Tank 2 was opened using detonation belt, in order to find the "theoretical" mass of explosive, which would match the experimental values. By knowing the TNT mass of the detonation belt and comparing it to the TNT mass obtained from the correlation, we can have an estimation for the energy which contributes to the blast wave. From this exercise, we deduced that only 40% of the energy contained in the detonation belt contributes to the blast wave strength.

- Performing similar analysis, but this time using the experimental results of helium-filled Tank 1 explosion, we can estimate the part of the mechanical energy devoted to the blast wave strength, which is close to the 45% of the initial mechanical energy, the other part being lost on fragments projection. We mention that the initial mechanical energy was multiplied by 1.8 due to the ground reflection (see [15] and references therein).

- As the last step, we used the same analysis for the test with hydrogen-filled tank. Based on the above estimations, we take 40% of the energy contained in the detonation belt, 45% of the initial mechanical energy and varied the fraction of chemical energy contributing to the blast wave

maximum overpressure. These estimations served as inputs for the correlation of [16] and the resulting maximum overpressures were systematically compared with the experimental data. For the present test, the fraction of the chemical energy was estimated at 12% (see Table 3).

Table 3. Values of the experimental and theoretical overpressures for the hydrogen explosion test

Distance from explosion (m)	142.5	205.0
Max. overpressure, exp. (mbar)	**64.1**	**60.2**
Max. overpressure (mbar), correl. of [16]; 8% of chemical energy	57.6	49.1
Max. overpressure (mbar), correl. of [16]; 10% of chemical energy	61.8	52.8
Max. overpressure (mbar), correl. of [16]; 12% of chemical energy	66.1	56.0

Fireball analysis

The behavior of the fireball is important to estimate the consequences of the ignition of the hydrogen following the sudden opening of the tank. It is particularly interesting to know the propagation velocity of the reactive wave. First, we have the line of thermocouples located along the axis of the tunnel near the ceiling. As shown in Figure 13 (left), the thermocouples' response allows us to identify two regimes: the first one is probably reactive over about ten meters with an average velocity of about 25 m/s (1) and the second one corresponds to the convection of the burnt gas cloud by the flow in the tunnel (2). In this test, the straw walls were no longer in place and the flow velocity was about 3.5 m/s from the bottom to the top of the tunnel.

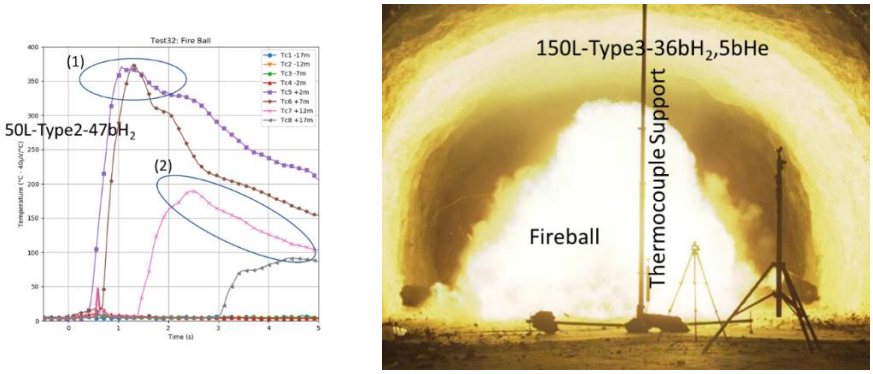

Figure 13. Fireball propagation along the tunnel ceiling.

The images of the explosion taken with the high-speed camera also allow us to analyze the dynamics of the fireball (Figure 13 - right). By processing the images (Figure 14 - left), it is possible to obtain the temporal evolution of an arbitrarily chosen interface (grey level - Figure 14 right). A kind of breathing of the fireball is clearly visible. That is to say, under the effect of the walls, the pressure waves are reflected and either accelerate or slow down the reactive wave. The characteristic time of this phenomenon is about 25 ms.

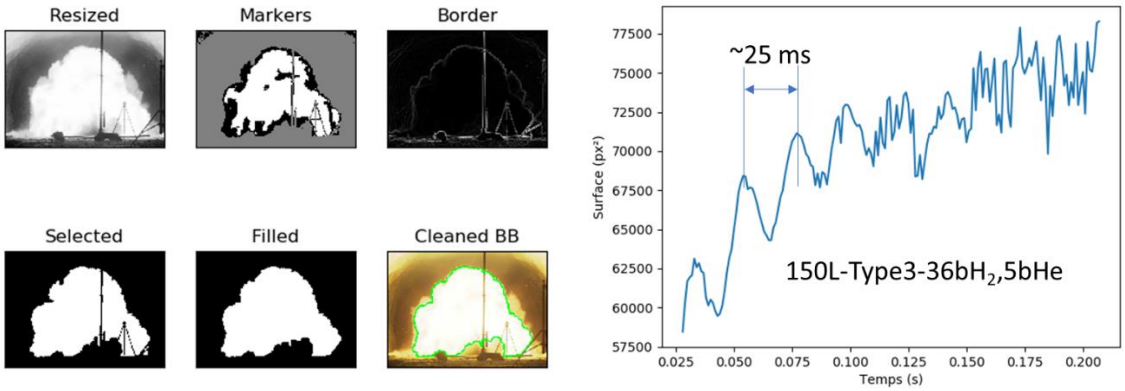

Figure 14. Fireball analysis (left) and its temporal evolution (right).

4.0 CONCLUSIONS AND PERSPECTIVES

In this paper we describe the results of preliminary tests which were conducted in the Tunnel du Mortier located in the commune of Autrans in the Vercors, France. Two scenarios were investigated, (a) jet fire evolution following the activation of TPRD due to conventional fuel car fire, and (b) explosion of compressed hydrogen tank. The obtained experimental data are compared to existing engineering correlations. Concerning the jet fire evolution the comparison of the flame length with recent correlations gives acceptable results. The radiative heat flux is better predicted while using the multipoint source model. As of the hydrogen tank explosion test, the fraction of chemical energy contributing to the blast wave strength is estimated using multi-step approach which includes analysis of the tank fragment explosion, helium-filled tank explosion and systematic application of correlation of [16]. The value of this fraction, 12%, is similar to the values estimated using CFD simulations in [15].

The hydrogen pressure range in these preliminary tests has been lowered down to 200 bar for jet fire tests and to 40-47 bar for tank explosion tests in order to verify the capability of various large-scale measurement techniques before scaling up to 70 Mpa, the subject of the second experimental campaign. The results of the present and of the second campaign will be used for benchmarking studies using engineering correlations and CFD codes.

REFERENCES

[1] W. G. Houf, G. H. Evans, E. Merilo, M. Groethe, and S. C. James, “Releases from hydrogen fuel-cell vehicles in tunnels,” *11th China Hydrog. Energy Conf.*, vol. 37, no. 1, pp. 715–719, Jan. 2012, doi: 10.1016/j.ijhydene.2011.09.110.

[2] Y. Sato *et al.*, “Hydrogen Release Deflagrations in a Sub-Scale Vehicle Tunnel,” presented at the World Hydrogen Energy Conference WHEC 16, Lyon, France, 2006.

[3] M. Groethe, E. Merilo, J. Colton, S. Chiba, Y. Sato, and H. Iwabuchi, “Large-scale hydrogen deflagrations and detonations,” *ICHS-2005*, vol. 32, no. 13, pp. 2125–2133, Sep. 2007, doi: 10.1016/j.ijhydene.2007.04.016.

[4] A. G. Venetsanos, D. Baraldi, P. Adams, P. S. Heggem, and H. Wilkening, “CFD modelling of hydrogen release, dispersion and combustion for automotive scenarios,” *Hydrog. Saf.*, vol. 21, no. 2, pp. 162–184, Mar. 2008, doi: 10.1016/j.jlp.2007.06.016.

[5] P. Middha and O. R. Hansen, “CFD simulation study to investigate the risk from hydrogen vehicles in tunnels,” *2nd Int. Conf. Hydrog. Saf.*, vol. 34, no. 14, pp. 5875–5886, Jul. 2009, doi: 10.1016/j.ijhydene.2009.02.004.

[6] H. Y. Bie and Z. R. Hao, “Simulation analysis on the risk of hydrogen releases and combustion in subsea tunnels,” *Spec. Issue 6th Int. Conf. Hydrog. Saf. ICHS 2015 19-21 Oct. 2015 Yokohama Jpn.*, vol. 42, no. 11, pp. 7617–7624, Mar. 2017, doi: 10.1016/j.ijhydene.2016.05.263.

[7] Y. Li *et al.*, “Numerical analysis of hydrogen release, dispersion and combustion in a tunnel with fuel cell vehicles using all-speed CFD code GASFLOW-MPI,” *Int. J. Hydrog. Energy*, Oct. 2020, doi: 10.1016/j.ijhydene.2020.09.063.
[8] V. Molkov and J.-B. Saffers, “Hydrogen jet flames,” *Int. J. Hydrog. Energy*, vol. 38, no. 19, pp. 8141–8158, Jun. 2013, doi: 10.1016/j.ijhydene.2012.08.106.
[9] C. Proust, D. Jamois, and E. Studer, “High pressure hydrogen fires,” *Int. J. Hydrog. Energy*, vol. 36, no. 3, pp. 2367–2373, 2010.
[10] E. Studer, D. Jamois, S. Jallais, G. Leroy, J. Hébrad, and V. Blanchetière, “Properties of large-scale hydrogen/methane jet fires,” *Int. J. Hydrog. Energy*, vol. 34, no. 23, pp. 9611–9619, 2009.
[11] M. Kuznetsov, S. Shentov, S. L. Brennan, and V. Molkov, “Experimental and Analytical Study of Hydrogen Jet Fire in a Vented Enclosure,” in *Proceedings of the Eighth International Seminar on Fire and Explosion Hazards (ISFEH8)*, Heifei, China, 2016, pp. 658–668, doi: 10.20285/c.sklfs.8thISFEH.066.
[12] R. W. Schefer, T. C. Houf W. G. and Williams, B. Bourne, and J. Colton, “Characterization of high pressure, underexpanded hydrogen-jet flames,” *Int. J. Hydrog. Energy*, vol. 32, no. 12, pp. 2081–2094, 2007.
[13] R. W. Schefer, W. G. Houf, B. Bourne, and J. Colton, “Spatial and radiative properties of an open-flame hydrogen plume,” *Int. J. Hydrog. Energy*, vol. 31, pp. 1332–1340, 2006.
[14] G. Hankinson and B. J. Lowesmith, “A consideration of methods of determining the radiative characteristics of jet fires,” *Combust. Flame*, vol. 159, no. 3, pp. 1165–1177, Mar. 2012, doi: 10.1016/j.combustflame.2011.09.004.
[15] V. Molkov and W. Dery, “The blast wave decay correlation for hydrogen tank rupture in a tunnel fire,” *Int. J. Hydrog. Energy*, vol. 45, no. 55, pp. 31289–31302, Nov. 2020, doi: 10.1016/j.ijhydene.2020.08.062.
[16] M. Silvestrini, B. Genova, and F. J. Leon Trujillo, “Energy concentration factor. A simple concept for the prediction of blast propagation in partially confined geometries,” *J. Loss Prev. Process Ind.*, vol. 22, no. 4, pp. 449–454, Jul. 2009, doi: 10.1016/j.jlp.2009.02.018.